Use of a digitally reconstructed radiograph-based computer simulation for the optimisation of chest radiographic techniques for computed radiography imaging systems

[1,3]C S MOORE, BSc, MSc, [2]G AVERY, MSc, FRCR, [2]S BALCAM, DCR(R), PGCert, [2]L NEEDLER, BSc, PGCert, [2]A SWIFT, MB ChB, FRCR, [1,3,5]A W BEAVIS, BSc, PhD and [1,4]J R SAUNDERSON, BSc, MSc

[1]*Radiation Physics Department, Queen's Centre for Oncology and Haematology, Hull, UK,* [2]*Radiology Department, Castle Hill Hospital, Hull and East Yorkshire Hospitals NHS Trust, Hull, UK,* [3]*Department of Computer Science, Faculty of Science, University of Hull, Hull, UK,* [4]*Postgraduate Medical Institute, University of Hull, Hull, UK, and* [5]*Faculty of Health and Wellbeing, Sheffield Hallam University, City Campus, Sheffield, UK*

Objectives: The purpose of this study was to derive an optimum radiographic technique for computed radiography (CR) chest imaging using a digitally reconstructed radiograph computer simulator. The simulator is capable of producing CR chest radiographs of adults with various tube potentials, receptor doses and scatter rejection.
Methods: Four experienced image evaluators graded images of average and obese adult patients at different potentials (average-sized, $n=50$; obese, $n=20$), receptor doses ($n=10$) and scatter rejection techniques (average-sized, $n=20$; obese, $n=20$). The quality of the images was evaluated using visually graded analysis. The influence of rib contrast was also assessed.
Results: For average-sized patients, image quality improved when tube potential was reduced compared with the reference (102 kVp). No scatter rejection was indicated. For obese patients, it has been shown that an antiscatter grid is indicated, and should be used in conjunction with as low a tube potential as possible (while allowing exposure times <20 ms). It is also possible to reduce receptor air kerma by 50% without adversely influencing image quality. Rib contrast did not interfere at any tube potential.
Conclusions: A virtual clinical trial has been performed with simulated chest CR images. Results indicate that low tube potentials (<102 kVp) are optimal for average and obese adults, the former acquired without scatter rejection, the latter with an anti-scatter grid. Lower receptor (and therefore patient doses) than those used clinically are possible while maintaining adequate image quality.

Received 8 March 2011
Revised 18 May 2011
Accepted 31 May 2011

DOI: 10.1259/bjr/47377285

Chest radiography is one of the most frequently performed diagnostic radiographic examinations in the UK owing to its value in the management of numerous clinical problems, such as the diagnosis of pulmonary diseases. A recent Health Protection Agency (HPA) report [1] presented the frequency and collective dose for medical and dental examinations in the UK in 2008, and demonstrated that chest radiographs contributed approximately 19.6% of all radiographic examinations (the second largest behind dental), although the contribution to collective dose was small at about 0.5%. It is a legal requirement in the UK under the Ionising Radiation (Medical Exposure) Regulations 2000 [2] to optimise all medical exposures. Because chest radiography is performed so frequently, optimisation of radiographic technique is an important research area, and has been investigated intensively in the literature.

Many investigators [3–12] have shown that projected patient anatomy is the limiting factor in chest radiography rather than system (including quantum) noise, and the term ''anatomical noise'' was derived from their work. It therefore follows that any images used to optimise a digital X-ray system for chest radiography must contain clinically realistic anatomical noise. Typically, work reported in the literature examining phosphor plate computed radiography (CR) chest optimisation has used relatively simple physical phantoms, which enable optimisation of parameters such as signal and noise but do not necessarily contain all the anatomical features (noise) required [13–17]. Our group has also investigated optimising a CR imaging system for chest radiography with a phantom containing only coarse anatomical detail [18–20], but how our conclusions related to the diagnostic quality of the clinical image was undetermined. More recently, several groups have used a computerised voxel phantom in Monte Carlo studies [21–25] in an attempt to model anatomical features, but the resolution of this voxel phantom [26] is relatively coarse (approximately 4 mm long×3 mm wide×3 mm thick) and is therefore likely to produce images of much lower spatial resolution than a real CR image (typical pixel pitch 0.1×0.1 mm). Another disadvantage of this Monte Carlo phantom is that it simulates only four tissue types (soft tissue, bone, bone

Address correspondence to: Mr Craig Moore, Radiation Physics Department, Princess Royal Hospital, Hull and East Yorkshire Hospitals NHS Trust, Saltshouse Road, Hull HU8 9HE, UK. E-mail: craig.moore@hey.nhs.uk

marrow and lung tissue) and air, thereby limiting the contribution of anatomical noise.

In this study we have used computer-simulated chest images that contain clinically realistic projected anatomy (*i.e.* anatomical noise), produced at various tube potentials, receptor air kerma and scatter rejection methods, to optimise CR chest radiographic techniques. The computer model is based on a digitally reconstructed radiograph (DRR) simulation system—a computer simulation of a conventional two-dimensional (2D) radiograph created from CT data—and has been produced and thoroughly validated by our group [27]. The evaluation of simulated images was carried out by experienced image evaluators, and so this work presents the results of a virtual clinical trial. A brief synopsis of the computer model and how the images are produced is described below:

1. The virtual phantom is derived from the chest portion of real patient CT data sets. The voxel resolution of the phantom is 0.34×0.80×0.34 mm (width×height ×depth). This is superior to the resolution of the computerised voxel phantom used in Monte Carlo studies [26].
2. CT number is converted into linear attenuation coefficient (LAC) using formulae derived from the Gammex-RMI model 467 (Gammex-RMI, Nottingham, UK) tissue equivalent phantom. This is a solid water cylinder that contains 17 inserts, the attenuation properties of which mimic the range of attenuations of the various tissues found *in vivo*. This demonstrates an improvement over the computerised phantom used for Monte Carlo studies, which contains only four tissue types.
3. X-ray spectra are generated using the techniques of Birch and Marshall as described in IPEM report 78 [28].
4. X-ray pencil beams are projected through the CT data set using a ray-casting method of DRR production. A ray-casting method was used as this has been shown to provide superior image quality to other methods such as splatting [29–31]. X-rays are attenuated as they move through the CT data in an exponential manner. The intensity of photons at each energy emerging from the virtual phantom is calculated.
5. Energy absorbed in the virtual CR phosphor is then calculated and converted to CR pixel value. This is the raw DRR.
6. Frequency-dependent noise is added to the raw DRR using a slightly adapted method described by Bath et al [32].
7. Scatter measured experimentally (''scatter masks'') on a clinical CR system is added to the raw DRR. The following separate scatter masks were acquired:

    i. With no clinical scatter rejection (*i.e.* non-grid). The ratio of scattered radiation absorbed in the CR phosphor to that of total radiation at 60 kVp (the scatter factor, SF) ranged from 0.33 to 0.47 in the lung region and from 0.66 to 0.85 in the spine/diaphragm region. SFs at 150 kVp ranged from 0.39 to 0.53 in the lung and from 0.69 to 0.88 in the spine/diaphragm. These values are in general agreement with SFs measured by Floyd et al [33] in humans. There is little change in SF in the spine/diaphragm regions with change in tube potential, but the effect is slightly more pronounced in the lung. This is similar to that reported by Bowenkamp and Boldingh [34].
    ii. With an antiscatter grid (strips per mm=4; grid ratio=12). SFs were (on average) 40% lower in the lung (*i.e.* SF=0.13–0.19) and 48% lower in the spine/diaphragm (*i.e.* SF=0.26–0.34) when compared with SFs derived without scatter rejection (non-grid). This correlates with the scatter transmission factor of 0.14 derived using a 10-cm-thick solid water phantom reported by Fetterly and Schueler [35].
    iii. With a clinical air-gap technique. The size of the air gap used was 20 cm based on the advice of an expert radiographer (Jo Cook, 2010, personal communication). SFs ranged from 0.29 to 0.39 in the lung region and from 0.65 to 0.68 in the spine/diaphragm region.

The resulting DRR images were validated quantitatively with a chest phantom and real patient CR images. Signal-to-noise ratio (SNR) values of the DRR images in the lung, spine and diaphragm regions agreed to within 15% (mean=5%) across the diagnostic energy range when compared with the CR images. Histograms was similar in shape and the dynamic range of the DRR images (minimum and maximum pixel values) were within two standard deviations of the mean of the corresponding values in the CR images. Qualitative validation was carried out by expert image evaluators and they all agreed that the DRRs adequately simulated real CR images, and that they were acceptable to use for optimisation studies. As well as normal chest anatomy, the model includes artificially added lung nodules. Lung nodules were chosen as they are indicative of common malignant disease, such as cancer, and non-malignant diseases such as tuberculosis, pneumonia and sarcoidosis. Expert image evaluators were also asked to score out of 10 (1=definitely not, 10=definitely) whether the position and appearance of the nodules were realistic. The mean ($\pm$1 standard deviation) score was 7.8$\pm$1.2, thus validating the appearance and positioning of the nodules.

Methods and materials

Digitally reconstructed radiograph simulation model and computed radiography imaging system

The DRR simulation system is capable of simulating CR chest images of average and obese adults at various tube potentials and receptor air kerma values, and using different scatter rejection techniques. The DRR model is currently configured to simulate the Agfa CR-85 (Agfa, Peissenberg, Germany) reader with MD-4.0 plates (35 cm×43 cm, effective pixel pitch of 0.1 mm), X-rayed with a focus to receptor distance of 180 cm with a Philips Optimus Diagnost TH (Philips Medical Systems, Cleveland,

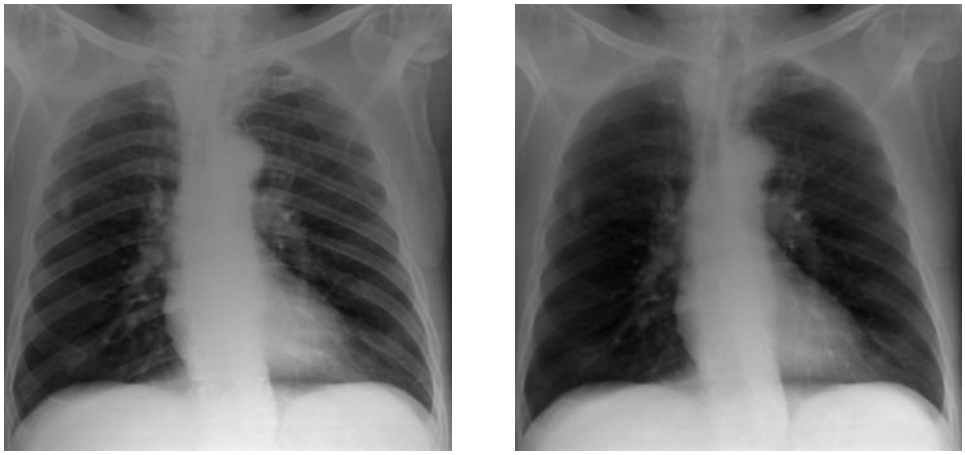

(a) (b)

Figure 1. Simulated chest images of an average-sized patient reconstructed at (a) 50 kVp and (b) 150 kVp.

OH) ceiling-suspended X-ray system, total inherent filtration equivalent to 3.1 mm of aluminium. Chest images produced by the DRR simulator reconstructed with tube potentials 50 and 150 kVp are shown in Figure 1a and Figure 1b, respectively. Figure 2a and Figure 2b show images reconstructed, respectively, with and without an antiscatter grid for scatter rejection (both 70 kVp). Finally, Figure 3a and Figure 3b present images at clinical receptor air kermas of, respectively, 7 and 2 μGy through the lung region (both 70 kVp).

As illustrated in Figure 1, contrast decreases as the tube potential increases, especially in the lung and ribs. This is of course expected because there is a decrease in differences between the linear attenuation coefficients of different human tissues with an increase in voltage, as the photoelectric cross-section varies with energy as approximately E^{-3}. Figure 2 demonstrates the effect of using an oscillating focused antiscatter grid (strips per millimetre=4; grid ratio=12), the detail in the spine and diaphragm regions being more visible with the grid. Finally, Figure 3 shows a higher level of noise in the heart region for the lower-dose image (Figure 3b) compared with the higher-dose image (Figure 3a).

Chest image reconstruction

The DRR simulator was used to reconstruct images to the following seven criteria (referred to hereafter as criteria 1–7):

1. CT data sets from 50 average-sized patients (70 ± 10 kg) were used to create simulated CR images. The images were simulated without any scatter rejection and at 11 different tube potentials from 50 to 150 kVp in approximate steps of 10 kVp (exact steps of 10 kVp were not possible on the clinical system and therefore not used in the simulation). Each image was reconstructed with a matched effective dose of 0.013 mSv ($\pm 1\%$) by using the clinical dose area product (DAP) value and therefore tube current–time product required at each tube potential to provide this effective dose. The computer model uses the milliampere value to calculate the intensity of X-ray photons incident on the virtual patient. DAP values were calculated using the effective dose calculation software PCXMC [36] and are shown in Table 1 along with corresponding milliampere values. The technique with no scatter rejection described here is

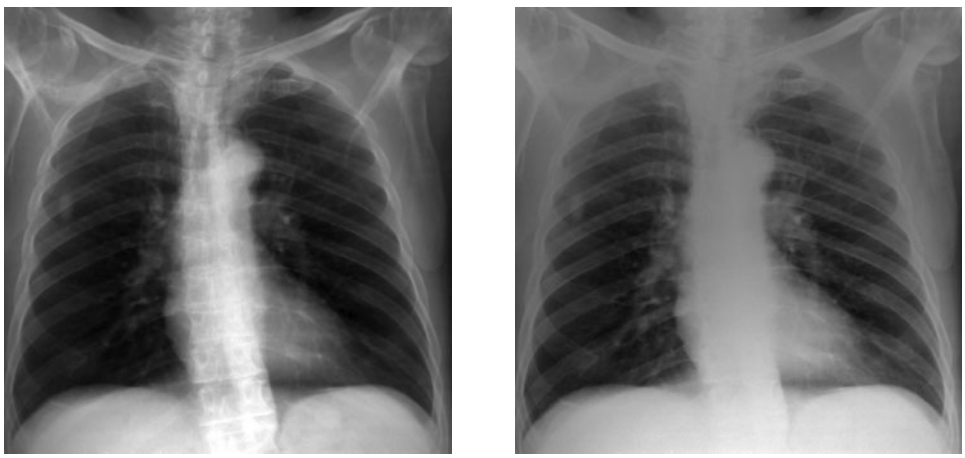

(a) (b)

Figure 2. Simulated chest images of an average-sized patient reconstructed (a) with and (b) without an antiscatter grid.

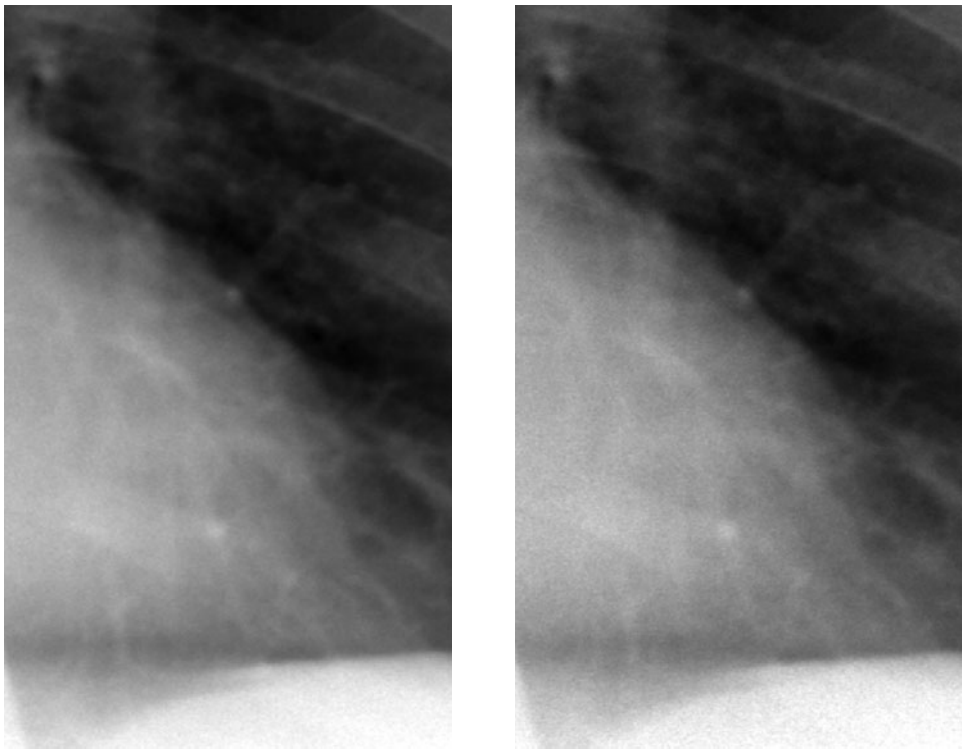

(a) (b)

Figure 3. Simulated chest images of an average-sized patient (heart region only) reconstructed at (a) 7 μGy and (b) 2 μGy.

consistent with the current chest imaging protocol used in our radiology department.

2. CT data sets from 20 average-sized patients were used to create simulated CR images with an oscillating focused antiscatter grid (strips per millimetre=4; grid ratio=12) focused at 140 cm focus-to-detector distance (FDD; useful range, 115–180 cm) incorporated into the model, each patient DRR set containing five images, each of a different tube voltage: 60, 81, 102, 125 and 141 kVp. Fewer images per patient were used on the advice of the image evaluators following their evaluations of criterion 1, as it became time-consuming to score numerous patients and difficult to differentiate differences in image quality in steps of 10 kVp. Each image was reconstructed with a matched effective dose.
3. CT data sets from 20 average-sized patients were used to create simulated CR images with an air gap antiscatter technique incorporated into the model, each patient DRR set containing five images, each of a different tube voltage: 60, 81, 102, 125 and 141 kVp. Each image was reconstructed with a matched effective dose.
4. Criteria 1–3 were repeated, but for obese patients, with matched effective doses 0.022, 0.10 and 0.03 mSv, respectively; the increase in dose being required for imaging of obese patients.
5. 10 average-sized patients, each containing images produced with varying receptor air kerma values through the lung region: 4.0, 3.0, 2.0, 1.5, 1.0 and 0.5 μGy.
6. 10 average-sized patients, each containing three images: an image reconstructed without any scatter rejection, an image reconstructed with an antiscatter grid and an image reconstructed with the air gap technique. The three images within each patient were reconstructed with the same tube potential, but each patient was reconstructed with a different potential (from patient 1=50 kVp to patient 10=150 kVp).
7. As for criterion 6, but for obese rather than average-sized patients.

Table 1. The exposure settings used to reconstruct each image for a matched effective dose of 0.013 mSv. The milliampere value is required for image reconstruction

Tube potential (kVp)	DAP (mGy cm^{-2})	Tube current-time product (mAs)
50	179	25
60	134	10
70	109	6.4
81	91	4
90	81	2.5
102	72	2
109	68	1.6
125	61	1.3
133	59	1
141	57	0.8
150	55	0.7

DAP, dose–area product.

Images of a given patient were attached in series to a single study and given the name CR_Patient_N, where N was the sequential patient number. For example, patient 1 had 11 series (images 50–150 kVp; see Table 1) and this study was called CR_Patient_1. The study was sent to the picture archiving and communications system (PACS)

network for observer evaluation. All other patients were subsequently reconstructed, named and sent to the PACS in the same manner.

Evaluation of clinical image quality

The Council of European Communities (CEC) Quality Criteria [37] defines important anatomical and image details for various diagnostic examinations, including chest radiography. The image criteria described in the CEC document, slightly revised [38–42] to reflect modern diagnostic requirements and previous experiences of other groups, were used to define anatomical features in each chest image for evaluation. As well as general chest structures, lung abnormalities were simulated in each image and evaluated, and are shown in Table 2. Four experienced image evaluators (two radiologists and two reporting radiographers) evaluated and graded the images on a reporting PACS workstation with a dual monitor configuration (Barco Ltd, Brussels, Belgium). The monitors were calibrated to national standards [43] and were kept in dedicated viewing rooms with lighting levels maintained at an acceptable level. The evaluators were asked to keep the final image in the series of each patient on the right-hand screen, as this was the reference image for grading (for example, assuming 11 images per patient, image 11 was kept on the right-hand screen). All other images (the ''test images'') were displayed in turn on the left-hand screen and graded against the reference image. For the tube potential optimisation studies (*i.e.* criteria 1–4), the reference image was reconstructed with a tube potential of 102 kVp. This reference tube potential was chosen because it is at the centre of the diagnostic energy range; our radiology department does not currently have a standard tube potential for chest radiography so a reference value based on local protocol could not be ascertained. None of the evaluators had any knowledge of what tube potential the test or reference images represented. Test images were also presented in a random order. Evaluators were allowed to change the window and level settings of each image prior to grading to optimise the appearance of each, as per clinical technique. For the scatter rejection study (criteria 6 and 7) the image derived without any scatter rejection was held as the reference image.

The evaluators graded the images using a visual grading analysis (VGA) system that has been used by Tingberg and Sjostrom [40] in a similar study using a physical chest phantom. The VGA method has been analysed and validated as an appropriate method to assess the image quality of chest radiographs by Tingberg [38], Mansson [44, 45] and Sund et al [46]. The image quality for six structures mentioned in the CEC document [37], as well as lung abnormalities in the hilar and lateral lung regions in each of the test images (see Table 2), was compared with the reference image on a scale incorporating seven points, as shown in Table 3. Ribs have been shown to be a general distraction for radiologists during the diagnostic interpretation of chest images [47], even if they are not overlying or close to lung nodules. Therefore image evaluators were also asked a simple ''yes/no'' question as to whether the ribs were an interference in the image. This work differs from previous VGA studies in that we have also included lung nodules as well as general chest structures.

For each image, a VGA score (VGAS) was calculated using the equation described by Tingberg and Sjostrom [40]:

$$\mathrm{VGAS} = \frac{\sum_{i=1}^{I}\sum_{s=1}^{S}\sum_{o=1}^{O} G_{\mathrm{I,S,O}}}{I \times S \times O} \quad (1)$$

where $G_{i,s,o}$ is the grading (−3, −2, −1, 0, +1, +2, +3) given by observer o for image i and structure s, I is the number of images per tube potential (dependent on number of patients), S is the number of structures (eight in total—six general and two abnormal) and O is the number of evaluators (four in this study). Negative and positive scores indicate inferior and superior image quality, respectively, in the test image compared with the reference image (see Table 3).

Scoring of the dose optimisation study (criterion 5) differed from the above as evaluators were simply asked to give yes/no answers to whether various regions in the chest image were diagnostically acceptable, as shown in Table 4. Also, during the study to determine whether scatter rejection would be beneficial (criteria 6 and 7), as well as VGA scores, image evaluators were asked to answer yes/no to the following question: ''Image 1 (test image) is at least 1.5 times the dose of image 3 (reference image). If image quality of image 1 is 'better' than image 3, does it still justify the large increase in dose?''

Statistical analysis

The results in this paper were tested for significance, firstly using the analysis of variance (ANOVA) test to examine interobserver variability, and then using the Student's *t*-test to examine differences between mean

Table 2. The chest structures used for visual grading analysis. Structures 1–6 are mentioned in the Council of European Communities (CEC) document [37]

Grading	Structure in CEC Guidance
1	Vessels seen 3 cm from the pleural margin
2	Thoracic vertebrae behind the heart
3	Retrocardiac vessels
4	Pleural margin
5	Vessels seen en face in the central lung region
6	Hilar region
	Other criteria
7	Abnormality in the lateral pulmonary region
8	Abnormality in the hilar region
9	Are the ribs a distraction? Yes/no

Table 3. The grading system for visual grading analysis

Grading	Visibility of structure
−3	Definitely inferior to the reference image
−2	Reasonably inferior to the reference image
−1	Slightly inferior to the reference image
0	Equal to the reference image
+1	Slightly better than the reference image
+2	Reasonably better than the reference image
+3	Definitely better than the reference image

Table 4. Chest structures/regions scored for receptor air kerma optimisation study. Each image was reconstructed with a different receptor air kerma, up to image N

Normal anatomy	Image 1	Image 2	Image N
Lung region: diagnostically acceptable? Yes/no			
Spine region: diagnostically acceptable? Yes/no			
Diaphragm region: diagnostically acceptable? Yes/no			
Abnormal structures			
Abnormalities: is lateral pulmonary region visible? Yes/no			
Abnormalities: is hilar region visible? Yes/no			

image quality scores (VGAS). A p-value of $<5\%$ was considered a statistically significant difference between data sets. Error bars shown in the graphical data of the results were calculated by averaging the standard deviations of each VGAS for each chest structure (Table 2) over all patients.

Phantom experiment to determine minimum possible X-ray exposure times

In the event the results demonstrate superior image quality with low tube potentials and antiscatter techniques we felt it necessary to determine whether a modern X-ray generator could produce exposure times of less than 20 ms as recommended in the CEC guidance. As such, the chest portion of the Alderson RANDO (Radiology Support Devices, Long Beach, CA) anthropomorphic phantom, consisting of a natural human skeleton embedded in a synthetic isocyanate rubber with lung substitute and air cavities, simulating the average male (approximately 73 kg), was set up on a Philips X–ray system as per local clinical chest protocol. Although primarily used for radiation therapy, RANDO has been shown to attenuate diagnostic energy radiation similar to that of water, which in turn has very similar properties to human muscle [48]. As the phantom only simulates the average adult, grocery store lard was added to the periphery to simulate obese fat (4 cm thickness was used, chosen on the advice of an expert radiographer; Andrew Stephens, 2010, personal communication). The phantom was exposed using tube potentials shown in Table 1, in sequential order, using milliamperes and corresponding time settings sufficient to produce lgM=2.00 $\pm$ 0.05. The lgM value is a receptor dose indicator displayed on the CR system for every image acquisition, which Agfa recommends should be 2.00 for a correctly exposed chest radiograph. After each exposure the CR phosphor plate (the same one was used for each exposure) was read through the CR reader.

Results and discussion

For all images evaluated in this study, the ANOVA test demonstrated a p-value of ≥ 0.08, and therefore it was deemed there was no significant difference between the scores of each image evaluator.

Image quality of 50 average-sized patients reconstructed without scatter rejection

The results of the optimisation study for 50 average patients reconstructed without scatter rejection (*i.e.* in the same manner as the chest radiographic technique currently used in our radiology department for average adults) are shown graphically in Figure 4.

It is clear from Figure 4 that the VGAS is higher for lower tube potential kilovolt potential settings, demonstrating image quality improves with a lower kilovolt potential. VGAS scores ranged from 0.41 for 50 kVp to 0.03 for 109 kVp, but there is very little difference between image quality at tube potentials greater than 102 kVp, as the VGAS ranged from 0.03 at 109 kVp to 0.07 at 150 kVp. Although there is a trend towards increased image quality at low tube potentials ($r^2>0.71$), it was only possible to statistically distinguish between 50 and 90 kVp ($p=0.033$), 80 and 90 kVp ($p=0.033$), and 80 and 109 kVp ($p=0.034$). All other combinations demonstrated p-values ≥ 0.102. Nevertheless, these results show that for matched effective dose, image quality improves with lower tube potentials, which is similar to results reported in the literature [13, 14, 24]. However, in lowering tube potential, an increase in milliamperes would be needed to compensate the reduced intensity of X-ray photons.

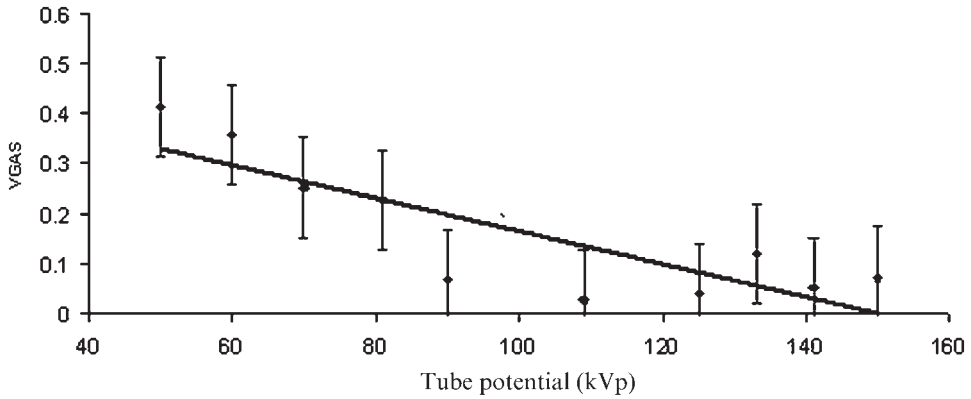

Figure 4. Image quality (visual grading analysis score; VGAS) results for average-sized patients reconstructed without any scatter rejection and matched effective dose.

This is likely to necessitate increased exposure times. This is discussed below.

Image quality of 20 average-sized patients reconstructed with an antiscatter grid

The results (figure not shown) for average patients reconstructed with an antiscatter grid modelled into the simulator demonstrate that there is a weak trend (r^2>0.58) towards increased image quality to low tube potentials, as per results above. VGAS results ranged from +0.039 (60 kVp) to −0.279 (141 kVp). However, there was no statistically significant difference between any of the observations ($p \geq 0.07$).

Image quality of 20 average-sized patients reconstructed with an air gap technique

The results (figure not shown) for average patients reconstructed with an air gap antiscatter technique modelled into the simulator demonstrate that there is a trend (r^2>0.78) towards increased image quality to higher tube potentials. VGAS results ranged from −0.297 (60 kVp) to +0.004 (125 kVp) and were all negative (except 125 kVp), suggesting all of the tube potentials were slightly inferior to 102 kVp. However, there was no statistically significant difference between any of the observations ($p \geq 0.08$).

Image quality of 20 obese patients reconstructed without scatter rejection methods

Figure 5 shows the results for overweight patients reconstructed without any scatter rejection modelled into the simulator.

There is a trend (r^2>0.73) towards increased image quality to higher tube potentials, demonstrating that all of the tube potentials performed approximately equally (minimum VGAS=−0.088; maximum VGAS=+0.02). There was no statistically significant difference between any of the observations ($p \geq 0.06$). Lower tube potentials probably perform worse than higher potentials because of relatively poor radiation penetration. Increased scatter from the obese patient, relative to the average patient, will also reduce image quality. It is likely that poor penetration and increased scatter in obese patients outweighs the benefits of inherent image contrast due to photoelectric absorption, even at lower tube potentials. It should be remembered that the mean scatter fraction (*i.e.* the ratio of scatter to total radiation incident at the image receptor) in chest radiography changes very little with tube potential [34, 49], and so the poorer image quality seen here at lower tube potentials depends more on patient size than on beam quality.

Image quality of 20 obese patients reconstructed with an anti-scatter grid

The results (figure not shown) for obese patients reconstructed with an antiscatter grid modelled into the simulator demonstrate that there is a strong trend (r^2>0.95) towards increased image quality at low tube potentials. VGAS results ranged from +0.61 (60 kVp) to −0.330 (141 kVp) and there were clinically significant differences between tube potentials 60 and 141 kVp (p<0.029), 81 and 141 kVp (p<0.012), and 125 and 141 kVp (p<0.017). These results suggest that if there is any advantage in using antiscatter grids for obese patients (see below), the lower the tube potential the better, and those lower than the reference (102 kVp) would provide superior image quality. However, as introduced above, low tube potentials will increase exposure times, but this is addressed further below.

Image quality of 20 obese patients reconstructed with an air gap technique

The results (figure not shown) for obese patients reconstructed with an air gap antiscatter rejection

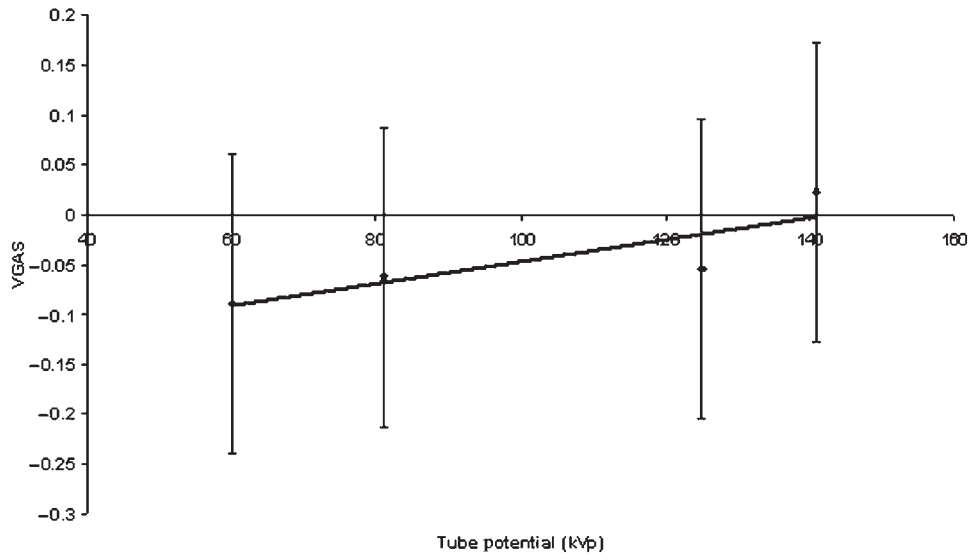

Figure 5. Image quality visual grading analysis score; VGAS results for obese patients reconstructed without any scatter rejection and matched effective dose.

method modelled into the simulator demonstrate that there is a weak trend ($r^2>0.55$) towards increased image quality at higher tube potentials, but all average VGAS scores are negative, ranging from −1.42 (60 kVp) to −0.075 (141 kVp). These results suggest that image quality is not improved irrespective of the tube potential used. Tube potential 60 kVp was significantly different from all the others ($p\leq0.004$), but there was no significant difference between any others ($p\geq0.201$). Poorer image quality at low tube potential is probably due to the factors mentioned above for image quality of obese patients reconstructed without scatter rejection methods.

Antiscatter grid vs *air gap—average-sized patients*

The results demonstrated that image quality is superior using scatter rejection techniques, and a grid outperforms the air gap method. The grid was significantly different from air gap ($p<0.006$) and no scatter rejection ($p<0.0002$), but the air gap method was not significantly different from no scatter rejection ($p=0.06$). However, image evaluators gave a ''no'' response in 100% of the cases when asked if the increase in dose justified using an antiscatter technique. Therefore, scatter rejection methods are not indicated for average patients.

Antiscatter grid vs *air gap—obese patients*

The results are similar to those for average-sized patients, in that image quality is superior using scatter rejection techniques, and a grid outperforms the air gap technique. The grid method was significantly different from air gap ($p<0.0004$) and no scatter rejection ($p<0.0002$), and the air gap method was significantly different from no scatter rejection ($p<0.006$). Image evaluators gave a ''yes'' response to 100% of the patients reconstructed with an antiscatter grid (presented blindly) when asked if the increase in dose was justified, but gave a ''no'' response to 100% of the air gap patients. Therefore, use of an antiscatter grid is indicated for obese patients, but an air gap technique is not, and so the question of exposure times with lower tube potentials (results for image quality of obese patients reconstructed with an antiscatter grid deemed low tube potentials superior for such patients) becomes important.

Phantom experiment to determine minimum possible X-ray exposure times

The results demonstrated that when average RANDO was exposed without using a grid, it was possible to use a tube current of 630 mA and exposure times <20 ms to obtain a lgM of 2.00 ± 0.05 with all tube potentials. Therefore it is possible to use low tube potentials as indicated in this work for average patients. However, for obese RANDO imaged with a grid, it was only possible to achieve the 20 ms limit with 109 kVp at 180 cm FDD or 90 kVp at 115 cm FDD—the lower distance permitted for this focused grid.

Image quality of 10 patients reconstructed with different receptor air kerma values

The response of each image evaluator to the criteria in Table 4 was quite surprising in that all deemed image quality acceptable in the lung region down to 1 μGy (*i.e.* all answers were ''yes''). This is approximately one-quarter of the air kerma for patients exposed with our radiology department's current standard exposure protocol. However, image quality was not deemed acceptable in the spine and diaphragm regions for an air kerma (through the lung region) of 1.5 μGy for any of the structures and abnormalities mentioned in Table 4. This suggests that chest imaging can be carried out with at least a 50% decrease in receptor dose, and therefore patient dose (for a given X-ray beam quality), while maintaining image quality that is diagnostically acceptable. A similar result has recently been reported by Veldkamp et al [50].

Interference of rib contrast

Ribs interfered in approximately 5% of images reconstructed at 50 kVp, but in no other. It is therefore not a limiting factor in chest radiography.

Conclusions

A DRR-based computer simulation of CR chest radiographs that contain clinically realistic anatomical noise has been used to identify optimum radiographic techniques for CR chest radiography with an Agfa CR-85 imaging system and MD-4.0 phosphor plates. Simulated images scored by four experienced image evaluators have shown that for average adult patients low tube potentials (<102 kVp) and no scatter rejection provide superior image quality. However, it has been shown that for obese adult patients an oscillating focused antiscatter grid is indicated, and should be used in conjunction with as low a tube potential as possible, as this combination provides superior image quality to any other investigated during this study. Measurements with a chest phantom on a clinical X-ray system demonstrate that any tube potential used without a grid can be used for average patients to satisfy the 20-ms exposure time limit, but at least 90 kVp must be used for obese patients. It has also been shown that receptor air kerma through the lung region can be reduced to 1.5 μGy while maintaining an adequate level of image quality, and the influence of rib contrast interfering with image evaluation is minimal.

References

1. Hart D, Wall BF, Hillier MC, Shrimpton PC. Frequency and collective dose for medical and dental X-ray examinations in the UK 2008. Chilton, UK: Health Protection Agency; 2010.
2. Stationary Office. The Ionising Radiation (Medical Exposure) Regulations 2000. London, UK: The Stationary Office; 2000.
3. Bochud FO, Valley JF, Verdun FR, Hessler C, Schnyder P. Estimation of the noisy component of anatomical backgrounds. Med Phys 1999;26:1365–70.

4. Samei E, Flynn MJ, Eyler WR. Detection of subtle lung nodules: relative influence of quantum and anatomical noise on chest radiographs. Radiology 1999;213:727–34.
5. Samei E, Eyler W, Baron L. Effects of anatomical structure on signal detection. In: Beutel J, Kundel HL, Van Metter RL, eds. Handbook of medical imaging. Vol. 1. Physics and psychophysics. Bellingham, WA: SPIE Press; 2000. pp. 655–82.
6. Keelan BW, Topfer K, Yorkston J, Sehnert WJ, Ellinwood JS. Relative impact of detector noise and anatomical structure on lung nodule detection. Proc SPIE 2004;5372:230–41.
7. Sund P, Bath M, Kheddache S, Mansson LG. Comparison of visual grading analysis and determination of detective quantum efficiency for evaluation system performance in digital chest radiography. Eur Radiol 2004;14:48–58.
8. Hakansson M, Bath M, Borjesson S, Kheddache S, Johnsson AA, Mansson LG. Nodule detection in digital chest radiography: effect of system noise. Radiat Prot Dosim 2005;114:97–101.
9. Hakansson M, Bath M, Borjesson S, Kheddache S, Grahn A, Ruschin M, et al. Nodule detection in digital chest radiography: summary of the RADIUS chest trial. Radiat Prot Dosim 2005;114:114–20.
10. Bath M, Hakansson M, Borjesson S, Kheddache S, Grahn A, Bochud FO, et al. Nodule detection in digital chest radiography: introduction to the RADIUS chest trial. Radiat Prot Dosim 2005;114:85–91.
11. Bath M, Hakansson M, Borjesson S, Kheddache S, Grahn A, Bochud FO, et al. Nodule detection in digital chest radiography: part of image background acting as pure noise. Radiat Prot Dosim 2005;114:102–8.
12. Bath M, Hakansson M, Borjesson S, Hoeschen C, Tischenko O, Kheddache S, et al. Nodule detection in digital chest radiography: effect of anatomical noise. Radiat Prot Dosim 2005;114:109–13.
13. Dobbins JT, Rice JJ, Beam CA, Ravin CE. Threshold perception performance with computed and screen-film radiography: implications for chest radiography. Radiology 1992;183:179–87.
14. Chotas HG, Floyd CE, Dobbins JT, Ravin CE. Digital chest radiography with photostimulable phosphors: signal-to-noise ratio as a function if kilovoltage with matched exposure risk. Radiology 1993;186:395–8.
15. Nobuhiro O, Hajime N, Seiichi M, Kunihiro T, Katsumi N, Akira Y. Optimal beam quality for chest radiography. Invest Radiol 1996;31:126–31.
16. Tingberg A, Sjostrom D. Search for optimal tube voltage for image plate radiography. Invest Radiol 1996;31:126–31.
17. Honey ID, MacKenzie A, Evans DS. Investigation of optimum energies for chest imaging using film-screen and computed radiography. Br J Radiol 2005;78:422–7.
18. Moore CS, Liney GP, Beavis AW, Saunderson JR. A method to optimize the processing algorithm of a computed radiography system for chest radiography. Br J Radiol 2007;80:727–30.
19. Moore CS, Beavis AW, Saunderson JR. Investigation of optimum X-ray beam tube voltage and filtration for chest radiography with a computed radiography system. Br J Radiol 2008;81:771–7.
20. Moore CS, Beavis AW, Saunderson JR. Investigating the exposure class of a computed radiography system for optimisation of physical image quality for chest radiography. Br J Radiol 2009;82:705–10.
21. Launders JH, Cowen AR, Bury RF, Hawkridge P. Towards image quality, beam energy and effective dose optimisation in digital thoracic radiography. Eur Radiol 2001;11:870–5.
22. Sandborg M, McVey G, Dance DR, Persliden J, Alm Carlsson G. A voxel phantom based Monte Carlo computer program for optimisation of chest and lumber spine X ray imaging systems. Radiat Prot Dosim 2000;90:105–8.
23. Sandborg M, McVey G, Dance DR, Alm Carlsson G. Schemes for the optimization of chest radiography using a computer model of the patient and X-ray system. Med Phys 2001;28:2007–19.
24. Sandborg M, Tingberg A, Ullman G, Dance DR, Alm Carlsson G. Comparison of clinical and physical measures of image quality in chest and pelvis computed radiography at different tube voltages. Med Phys 2006;33:4169–75.
25. Ullman G, Sandborg S, Dance DR, Hunt RA, Carlsson GA. Towards optimization in digital chest radiography using Monte Carlo modelling. Phys Med Biol 2006;51:2729–43.
26. Zubal G, Harrell CR, Smith EO, Rattner Z, Gindi G, Hoffer PB. Computerized three-dimensional segmented human anatomy. Med Phys 1994;21:299–302.
27. Moore CS, Liney GP, Beavis AW, Saunderson JR. A method to produce and validate a digitally reconstructed radiograph-based computer simulation for optimization of chest radiographs acquired with a computed radiography imaging system. Br J Radiol 2011;84:890–902.
28. Sutton DG, Reilly AJ. Report 78 spectrum processor. York, UK: IPEM; 1997.
29. Milickovic N, Baltas D, Giannouli S, Lahanas M, Zamboglou N. CT imaging based digitally reconstructed radiographs and their application in brachytherapy. Phys Med Biol 2000;45:2787–800.
30. Cai W, Sakas G. DRR volume rendering using splatting in shear-warp context. Nuclear Science Proceedings IEEE 2001;3:12–17.
31. Westover LA. Interactive volume rendering. In: Proceedings of Volume Visualisation Workshop; Chapel Hill, NC; May 18–19. Chapel Hill, NC: Dept of Computer Science, University of North Carolina, 1989: 9–16.
32. Bath M, Hakansson M, Tingberg A, Mansson LG. Method of simulating dose reduction for digital radiographic systems. Radiat Prot Dosim 2005;114:253–9.
33. Floyd CE, Lo JY, Chotas HG, Ravin CE. Quantitative scatter measurement in digital radiography using a photostimulable phosphor imaging system. Med Phys 1991;18:408–13.
34. Bowenkamp JG, Boldingh WH. Quality and choice of Potter Bucky grids. I. A new method for the unambiguous determination of the quality of a grid. Acto Radiol 1959;51:479.
35. Fetterly KA, Schueler BA. Experimental evaluation of fibre-interspaced antiscatter grids for large patient imaging with digital X-ray systems. Phys Med Biol 2007;52:4863–80.
36. Radiation and Nuclear Safety Authority. PCXMC dose calculations, version 2.0.1. Helsinki, Finland: Radiation and Nuclear Safety Authority; 2008.
37. Council of the European Communities. European guidelines on quality criteria for diagnostic radiographic images. Report EUR 16260. Geneva, Switzerland: European Commission; 1996.
38. Tingberg A. Quantifying the quality of medical X-ray images. An evaluation based on normal anatomy for lumbar spine and chest radiography. Thesis, Lund University, Malmo, Sweden, 2000.
39. Sund P, Herrmann C, Tingberg A, Kheddache S, Mansson LG, Almen A, et al. Comparison of two methods for evaluating image quality of chest radiographs. Proc SPIE 2000;3981:251–7.
40. Tingberg A, Sjostrom D. Optimisation of image plate radiography with respect to tube voltage. Radiat Prot Dosim 2005;114:286–93.
41. Lanhede B, Bath M, Kheddache S, Sund P, Björneld L, Widell M, et al. The influence of different technique factors on image quality of chest radiographs as evaluated by modified CEC image quality criteria. Br J Radiol 2002;75:38–49.
42. Tingberg A, Herrmann C, Lanhede B, Almén A, Sandborg M, McVey G, et al. The influence of the characteristic curve on the image quality of clinical radiographs. Br J Radiol 2004;77:204–15.

43. Institute of Physics and Engineering in Medicine. Report 91: recommended standards for the routine performance testing of diagnostic X-ray imaging systems. York, UK: Institute of Physics and Engineering in Medicine; 2005.
44. Mansson LG. Evaluation of radiographic procedures, 1994. Investigations related to chest imaging. Thesis, Goteburg University, Goteburg.
45. Mansson LG. Methods for the evaluation of image quality: a review. Radiat Prot Dosim 2000;90:89–99.
46. Sund P, Herrmann C, Almen A, Mattsson S. Comparison of two methods for evaluating image quality in chest radiographs. *Proc SPIE* 2000;3977:437–43.
47. Hoeschen C, Tischenko O, Buhr E, Illers H. Comparison of technical and anatomical noise in digital thorax X-ray images. Radiat Prot Dosimetry 2005;114:75–80.
48. Shrimpton PC, Wall BF, Fisher ES. The tissue-equivalence of the Alderson-Rando anthropomorphic phantom for X-rays of diagnostic qualities. Phys Med Biol 1981;26:133–9.
49. Floyd CE, Baker JA, Lo JY, Ravin CE. Posterior beam stop method for scatter fraction measurement in digital radiography. Invest Radiol 1992;27:119–23.
50. Veldkamp JH, Kroft LJM, Geleijns J. Dose and perceived image quality in chest radiography. Eur J Radiol 2009; 72:209–17.